Analysis and modelling of the contact radius effect on the cutting forces in cylindrical and face turning of Ti6Al4V titanium alloy

Théo Dorlin[a,b]*, Guillaume Fromentin[a], Jean-Philippe Costes[a]

[a]*Arts et Metiers ParisTech, LaBoMaP, 71250 Cluny, France*
[b]*Safran S.A., Research & Technology Center, 78772 Magny-Les-Hameaux, France*

* Corresponding author. Tel.: +33-385-595-217; fax: +33-385-595-370. *E-mail address:* theo.dorlin@ensam.eu

Abstract

Cutting forces are representative data to characterize machining operations. They have to be known to perform the part manufacturing. Therefore, cutting forces predictive models are useful and it is possible to optimize them by taking into account new parameters. Hence, this study deals with the geometrical modelling of tool-workpiece interaction and its influence on the cutting forces. The analysis focuses on convex contact radius between the machined part and the tool. Experiments are based on cylindrical and face turning of Ti6Al4V titanium alloy. The results highlight a significant influence of contact conditions on ploughing mechanisms, and consequently on the cutting forces intensity. This phenomenon is taken into account in the suggested models, providing a better accuracy of cutting forces modelled.

Keywords: Cutting; Forces; Turning; Modelling; Ploughing; Titanum alloy;

1. Introduction

Current constraints in aeronautical industry lead to manufacture parts in "difficult-to-cut" materials like titanium alloys and with new complex geometries.

Nevertheless, some kinds of complex geometries could lead to highly flexible parts, sensitive to cutting forces. Thereby, unsuitable cutting forces could result in vibrations and deformations in finishing operations, or to an inappropriate machine tool spindle choice for roughing operations. Both are conditions for rejecting a high-value added machined part, or damaging machines, and so financial losses for the company. Since the objectives are to enhance the use of resources and to have no quality escape, the cutting forces have to be known precisely in order to predict deflections on the machined part, and in order to optimize the industrialization of manufactured parts on the machines.

In one hand, in order to have true values of cutting forces in turning operations, these forces have to be measured during cutting processes which lead to costly trials. In the other hand, since decades predictive models are developed by many authors in order to predict cutting forces. Although current models give a precise prediction, they may be optimised.

That is the reason why, the aim of the following research is to develop a more accurate predictive model for cutting forces based on few experimental trials. The added value of this modelling is the consideration of the "ploughing" effect influence on the cutting forces, linked to the clearance face contact radius, which is especially in relation with the piece diameter.

In fact, during material cutting (with $h >> r_\beta$) a major part of the uncut chip thickness is evacuated, as a chip, along the rake face, while the other portion is ploughed under the flank face. Most of current cutting forces predictive models are focusing on the modelling of primary shearing zone contribution to the cutting forces [1–4]. Despite the fact that, this contribution had been highlighted as the dominant one in multiple cases, Albrecht [5] noted that in the case of finishing operations, the contribution of the third shearing zone should not be neglected. These observations were confirmed by Wyen and Wegener [6], Ng [7], who refuted the linearity

relation between the cutting forces and the uncut chip thickness, for small values of uncut chip thickness, also called the "size-effect". Therefore many scientists focused theirs research on measuring the values of the ploughing force, as proposed by Stevenson, Popov and Dugin, who compared several methods [8–11]. Based on these conclusions the ploughing force was included in the cutting forces models as suggested by Huang and Liang or Kaymacki et al. [12,13]. However these formulations, relating the ploughing force to polynomial functions of the uncut chip thickness or the cutting speed, can be discussed. Indeed studies concerning the determination of ploughing force are often developed on planning tests, and so doesn't take into account the potential influence of the part diameter, as suggested by Germain or Campocasso et al. [14,15]. Therefore the purpose of this study is to enhance the modelling of the ploughing force by analysing the contact radius effect on cutting forces.

Nomenclature

a_p	depth of cut
α_n	tool normal clearance angle
f	feed per revolution
f_h	local normal force
f_v	local tangential force
F_c	global cutting force
F_f	global feed force
F_p	global penetration force
γ_n	tool normal rake angle
h	uncut chip thickness
κ_r	tool cutting edge lead angle
λ_s	tool cutting edge inclination angle
L_{seg}	segment length of the discretised cutting edge
Nb_{seg}	total number of segment used for discretisation
P_o	tool orthogonal plane
P_r	tool reference plane
r_β	rounded cutting edge radius
$R^o_{c,c}$	clearance face contact radius in tool orthogonal plane
r_ε	corner radius
R_m	machined part radius
θ	angle of the considered point on the cutting edge
V_B	flank wear of the cutting tool
V_c	cutting speed
V_f	feed speed
$\vec{X}_M$	radial axis (machine frame)
$\vec{Y}_M$	tangential axis (machine frame)
$\vec{Z}_M$	axial axis (machine frame)

The study declines into four sections. The first point is devoted to the experimental details. Then the second part illustrates the clearance face contact radius, seen in the tool orthogonal plane, as defined in the ISO 3002-1 standard [16], for the cases of cylindrical and face turning. Afterwards a direct analysis of the contact radius influence on cutting forces is realised, in cylindrical and face turning with a round insert tool. Based on these conclusions two mechanistic predictive models are established. Finally, thanks to an inverse identification method, trials in real conditions, in cylindrical and face turning, are realised to determine the values of the predictive model coefficients. The modelled cutting forces, from the suggested models and the model, commonly used and developed by Armarego [2], are compared to the measured cutting forces in order to evaluate the quality of the prediction provided by the new predictive models.

2. Experimental details

Experimental cutting for whole tests are realised on a instrumented 2-axis lathe, with numerical command, at a cutting speed V_c equal to 90 m/min and determined according to tool-material pair method, defined by the NF-E66-520-4 standard [17]. The work material used is a Ti6Al4V titanium alloy workpiece. The homogeneity was verified by micro-hardness tests from the heart of the workpiece to the surface. This material is machined assisted with a Blaser Blasocut 2000 CF coolant, at low pressure. The cutting tool used for the tests is the LCGR1705-500-RP Seco Tools MDT round insert, used for profiling operations. The geometry has been measured and specified in Table 1. The cutting forces acquisition has been gathered with a Kistler type 9121 piezoelectric dynamometer and a Kistler 5019A amplifier.

Table 1. Geometry of the LCGR1705-500-RP Seco Tool MDT insert on tool holder.

α_n (°)	γ_n (°)	λ_s (°)	r_β (µm)	r_ε (mm)
7	7	0	18	2.5

3. Clearance face contact radius in cylindrical and face turning

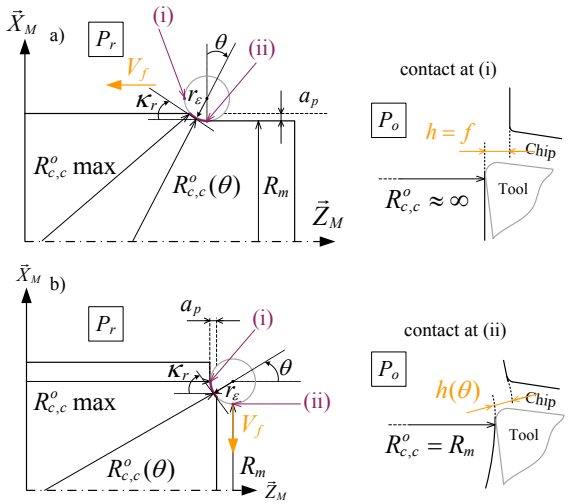

Fig. 1. Representation of the $R^o_{c,c}$ radius in the cases of (a) cylindrical turning; (b) face turning.

As shown in Fig. 1, the clearance face contact radius refers to the distance between the considered point on the cutting edge and the revolution axis of the part. The considered direction is the normal to the tangent to the cutting edge at the considered point.

This parameter is representative of the tool-workpiece interaction and it should be noted that the $R^o_{c,c}$ radius evolves drastically as a function of the depth of cut. As presented in Fig. 1, at the generating point (i.e. $\theta = 0°$) illustrated as (ii), the value of the $R^o_{c,c}$ radius is equal to the machined part radius. Whereas, for an operation in which the depth of cut is equal to the corner radius, at the higher point (i.e. $\theta = 90°$) illustrated as (i), the $R^o_{c,c}$ radius tends to infinity. The expression of this parameter is detailed in equation (1) in the case of a cylindrical turning operation, and by equation (2) in the case of a face turning operation.

$$R^o_{c,c} = r_\varepsilon \times \left(\frac{1}{cos(\theta)} - 1 \right) + \frac{R_m}{cos(\theta)} \quad (1)$$

$$R^o_{c,c} = r_\varepsilon \times \left(\frac{1}{sin(\theta)} - 1 \right) + \frac{R_m}{sin(\theta)} \quad (2)$$

As suggested by many authors in the case of a turning operation with a round insert (i.e. representative of a finishing operation in the tool nose), several geometrical parameters are not constant along the cutting edge engaged. It is the case of the uncut chip thickness [12], the cutting edge lead angle [15] but also the clearance face contact radius, as explained and presented in Fig. 2.

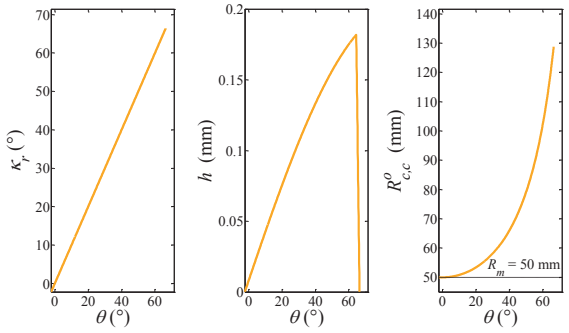

Fig. 2. Evolution of local parameters in cylindrical turning
($a_p = 1.5$ mm; $f = 0.2$ mm/rev; $r_\varepsilon = 2.5$ mm; $R_m = 50$ mm).

Therefore since the $R^o_{c,c}$ radius varies in large proportions along the cutting edge, its influence on cutting forces has to be evaluated. However as shown in Fig. 2, equations (1) and (2), the evolution of the $R^o_{c,c}$ radius is geometrically associated with the variation of the κ_r angle. In order to study the effect of the clearance face contact radius on cutting forces, independently from any other parameter, the hypothesis of a non-influence of the variation of the κ_r angle on cutting forces has been assumed.

4. Analysis of the contact radius effect on global forces in cylindrical turning and face turning

4.1. Cutting tests in cylindrical and face turning

In order to determine the influence of the $R^o_{c,c}$ radius on cutting forces, two experimental configurations have been carried out: cylindrical turning and face turning. Indeed as represented in Fig. 1, for a low value of depth of cut, at the same cross-section area and almost the same machine part radius, the two configurations present different ranges of variation for the $R^o_{c,c}$ radius along the cutting edge. This observation is illustrated in the Table 2.

Table 2. Comparison of the variation ranges of the $R^o_{c,c}$ radius provided by cylindrical and face turning, for the same cutting conditions ($a_p = 0.5$ mm; $r_\varepsilon = 2.5$ mm; $R_m = 50$ mm).

Turning config.	κ_r min. (°)	κ_r max. (°)	$R^o_{c,c}$ min. (mm)	$R^o_{c,c}$ max. (mm)
Cylindrical	-2.29	11.5	50	51.08
Face	-2.29	11.5	250	1310

So, the comparison of these two configurations leads to the direct analysis of the $R^o_{c,c}$ radius influence on global cutting forces.

Since it does exist a strong interaction between the cutting forces and the tool wear, each trial is realised during a short cutting length equivalent to 5 revolutions (i.e. 1 to engage the cutting tool, 3 revolutions in steady-state and 1 revolution for the cutting tool exit) in order to limit the influence of tool wear on the evolution of cutting forces during acquisition. The flank wear is observed with a microscope, according to principles defined in the ISO 3685 standard [18].

The values of presented cutting forces are the average of measurements realised during the 3 revolutions with the cutting tool engaged. Each trial is realised within the same titanium Ti6Al4V workpiece and the same Seco Tool MDT insert, in order to limit dispersions. Besides, each trial is also repeated in order to quantify the repeatability of the measurements. Lastly as illustrated in Fig. 3, the flank wear has been included in the experimental design under two levels in order to take into consideration the influence of the flank wear on the cutting forces measurements. Once the trials series with the new cutting edge is completed, the aim is to introduce a uniform and acceptable flank wear along the entire cutting edge (the limit in production is about $V_B = 300$ µm). Consequently, one test in cylindrical turning and one test in face turning have been realised during the same cutting length before collecting data for the second trials series. Therefore the flank wear is constant all along the cutting edge ($V_B = 100$ µm). The results are presented in Fig. 4 and Fig. 5.

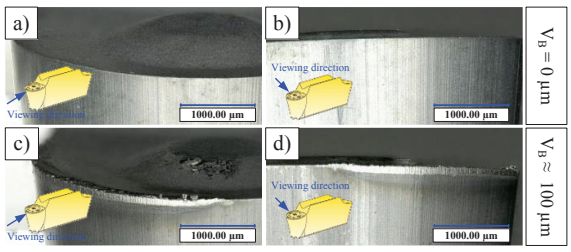

Fig. 3. Photographs of the two levels of flank wear (a) and (b) unworn cutting edge; (c) and (d) cutting edge with constant flank wear.

4.2. Results and observations

As explained in Fig. 4 and Fig. 5, the experiment design is developed under one small level of depth of cut, two levels of feed per revolution and two levels of flank wear in cylindrical and face turning. Fig. 4 presents the results obtained from the campaign with a new cutting edge, while Fig. 5 illustrates the results collected from the campaign with a worn cutting edge.

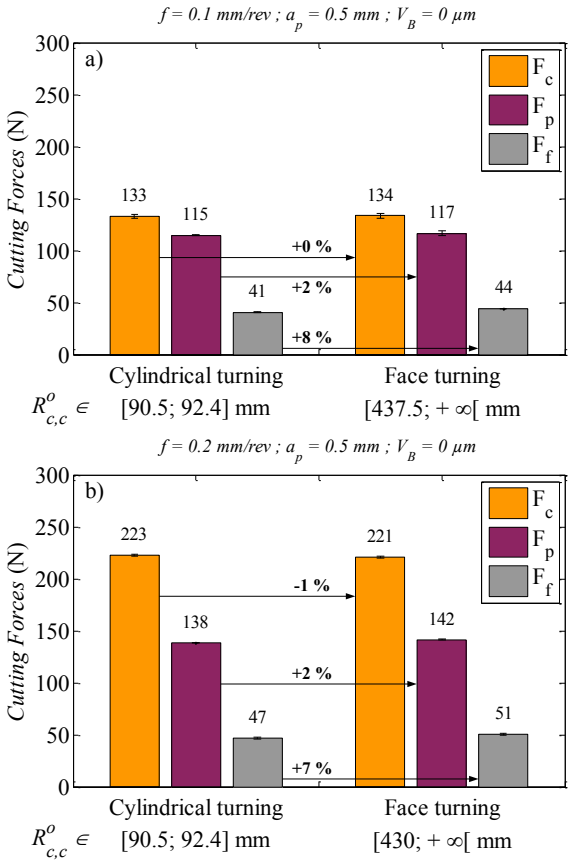

Fig. 4. Global cutting forces evolutions according to $R^o_{c,c}$ radius variation with new cutting edge ($V_B = 0$ µm).

According to Fig. 4, the first observation is that the clearance face radius seems to have an influence only on the global feed force. Others components do not present a significant variation with respect to the evolution of the $R^o_{c,c}$ contact radius. Concerning, the F_f global force, when the $R^o_{c,c}$ radius grows the intensity of this component rises too. This increase is about 7-8% between the cylindrical turning configuration and the face turning configuration. However the cutting force intensities for this component are very low. Although the cutting trials are repeatable, these observations are not sufficient to confirm that the effect of the $R^o_{c,c}$ radius does exist in the case of a new cutting edge.

Secondly, the tendencies presented by each component of the global cutting force are similar whatever the feed per revolution is. Therefore in the case of a new cutting edge, the potential effect of the $R^o_{c,c}$ radius on cutting forces is dissociated to the feed per revolution effect on cutting forces.

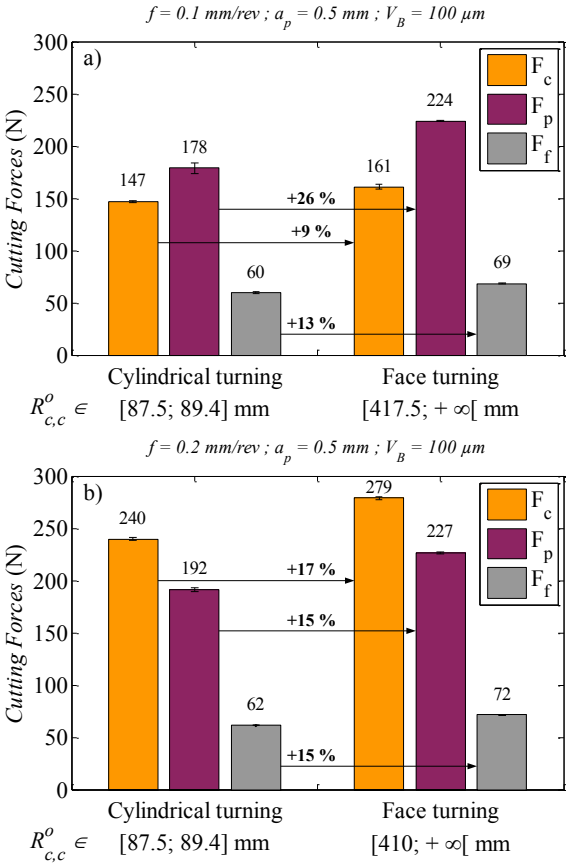

Fig. 5. Global cutting forces evolutions according to $R^o_{c,c}$ radius variation with worn cutting edge ($V_B = 100$ µm).

As illustrated by Fig. 5, the first observation is in accordance with the results observed at the Fig. 4, the trends presented by each components of the global cutting force are the same regardless of the feed per revolution value.

Secondly, in contrast with the observations made at the Fig. 4, in the case of a $V_B = 100$ µm, the effect of the $R^o_{c,c}$ radius is significant. Indeed the 3 components are increasing between the cylindrical turning configuration and the face turning configuration. The component F_c increases of 9 to 17%, while the increases regarding the two others components, F_p and F_f , are at least 13%.

Therefore it seems that the effect of the $R^o_{c,c}$ radius on the cutting forces increase with the flank wear. It confirms that the phenomenon causing cutting forces evolution lies in the flank face of the cutting tool.

Consequently the difference between the cutting forces magnitudes observed in cylindrical turning and face turning configurations seem to be explained, from a mechanistic point of view, by the variation of the clearance face contact radius. And so, this parameter has to be taken into account in modelling for a better accuracy.

5. Cutting force modelling: application to cylindrical turning and face turning

5.1. Form and calibration of suggested predictive models

In order to model the cutting force, in addition to the analysis presented in section 4, the discretisation method detailed in Fig. 6 and equations (3), (4) and (5), along with an inverse identification methodology are employed in case of a non-inclined cutting edge (i.e. $\lambda_s = 0°$).

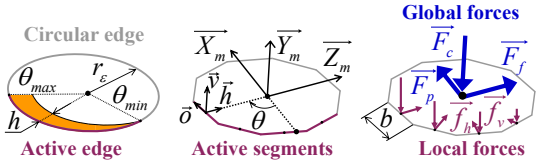

Fig. 6. Edge discretisation method, illustrated in the case of cylindrical turning with a round insert [15].

$$F_c = \sum_{i=1}^{Nb_{seg}} f_{v,i} \times L_{seg,i} \quad (3)$$

$$F_p = \sum_{i=1}^{Nb_{seg}} f_{h,i} \times \cos(\theta_i) \times L_{seg,i} \quad (4)$$

$$F_f = \sum_{i=1}^{Nb_{seg}} f_{h,i} \times \sin(\theta_i) \times L_{seg,i} \quad (5)$$

From a mechanical approach, in order to model cutting forces the uncut chip thickness has always been highlighted as a major parameter. Consequently, several predictive models, which include this parameter, have been developed. From a mechanistic point of view, Armarego and Epp [19] suggested a model presented in equation (6) with $j \in \{v;h\}$. Today, this model, commonly used is considered as a reference.

$$f_j = \underbrace{k_{j0}}_{\text{edge effect}} + \underbrace{k_{j1} \times h}_{\text{cutting effect}} \quad (6)$$

Based on previous conclusions, which suggested a ponderation of the edge effect, a local cutting force model has to be formalised. This should be in agreement with the increase of the cutting forces with respect to the growth of the $R^o_{c,c}$ radius and should converge to a finite value of cutting forces for an infinite value of $R^o_{c,c}$ radius (i.e. representative of a cutting operation in which $a_p = r_\varepsilon$). Consequently, two predictive models have been expressed via a phenomenological approach and are suggested in equations (7) and (8) with $j \in \{v;h\}$.

$$f_j = k_{j0} + k_{j2} \times exp\left(\frac{-k_{j3}}{R^o_{c,c}}\right) + k_{j1} \times h \quad (7)$$

$$f_j = k_{j0} + k_{j2} \times \arctan\left(k_{j3} \times (R^o_{c,c} - k_{j4})\right) + k_{j1} \times h \quad (8)$$

To determine the values of the unknown coefficients, 12 cutting trials are realised. The experimental plan presented in Table 3, should cover large ranges of variation of uncut chip thickness and $R^o_{c,c}$ radius in order to test the model in a large domain of validity. Moreover, thanks to the observations made at section 4.2, the whole cutting tests are realised in the case of an acceptable worn cutting edge (i.e. $V_B = 100$ µm).

Table 3. Experimental design for inverse identification cutting trials with $V_B = 100$ µm.

Turn. Config.	a_p (mm)	f (mm/r.)	$R^o_{c,c}$ min (mm)	$R^o_{c,c}$ max (mm)	Cutting forces (N) F_c	F_p	F_c
Cyl.	2.5	0.2	77	∞	1014	538	553
Cyl.	2.5	0.1	77	∞	654	528	543
Face	2.5	0.2	72	∞	1024	555	546
Face	2.5	0.1	71	∞	641	535	539
Cyl.	2	0.2	86	145	834	536	451
Cyl.	2	0.1	86	145	551	521	450
Face	1	0.2	142	1485	490	457	243
Face	1	0.1	146	3048	324	449	250
Cyl.	0.5	0.2	78	80	234	185	94
Cyl.	0.5	0.1	78	80	151	168	91
Face	0.5	0.2	285	1485	271	324	116
Face	0.5	0.1	281	2935	174	315	115

Thanks to an algorithm of inverse identification applicable to cylindrical and face turning operations, the unknown coefficients of the previous predictive models have been determined. All values are presented in Table 4.

Table 4. Values of predictive models coefficients, determined via inverse identification algorithm.

Armarego's model (6)			
k_{v0} (N/mm)		k_{v1} (N/mm²)	
63		1425	
k_{h0} (N/mm)		k_{h1} (N/mm²)	
1		792	
Exponential model (7)			
k_{v0} (N/mm)	k_{v1} (N/mm²)	k_{v2} (N/mm)	k_{v3} (mm)
-509238	1418	509324	$5*10^{-3}$
k_{h0} (N/mm)	k_{h1} (N/mm²)	k_{h2} (N/mm)	k_{h3} (mm)
1	-273	509519	$1*10^{-2}$
Arc tangential model (8)			
k_{v0} (N/mm)	k_{v1} (N/mm²)	k_{v2} (N/mm)	k_{v3} (mm^{-1})	k_{v4} (mm)
6342	1429	-3998	-9089	631642
k_{h0} (N/mm)	k_{h1} (N/mm²)	k_{h2} (N/mm)	k_{h3} (mm^{-1})	k_{h4} (mm)
1	-298	3893	370488	6

As presented in Table 4, the values of coefficients determined are the results of an unconstrained mathematical resolution. Therefore in few cases, some coefficients taken individually may not have a mathematical value in accordance with their physical meaning.

5.2. Comparison between predictive models

In order to highlight the value-added by the new cutting forces predictive models, a comparison with the prediction realised with the Armarego's model is presented in Table 5.

Table 5. Cutting forces modelling relative errors provided by the three predictive models.

	Relative error on each component (%)		
	F_c	F_p	F_f
Armarego's model (6)			
Min.	2	7	0
Max.	12	49	51
Average	**6**	**26**	**27**
Exponential model (7)			
Min.	1	0	0
Max.	9	10	20
Average	**4**	**4**	**6**
Arc tangential model (8)			
Min.	0	1	0
Max.	11	15	19
Average	**5**	**5**	**8**

As presented in Table 5, the prediction of the cutting force F_c is approximately the same regardless of which predictive model is employed. Nonetheless suggested predictive models are both enhancing greatly the prediction of the components F_p and F_f . In comparison with Armarego's model, the component F_f is modelled with a precision gain of, at least, 19 %. While the precision gain concerning the F_p component is about 21 %. These results are a major breakthrough because these two components are directly linked to part or tool deflections. Finally, the two suggested models, which include the $R_{c,c}^o$ radius effect on cutting forces, provide a better accuracy for 2 of 3 components, with a slight advantage for the exponential model (7).

6. Conclusion

The aim of this work is to optimize the prediction of cutting forces in turning of titanium alloy Ti6Al4V by taking into account the $R_{c,c}^o$ radius influence on cutting forces. Then two new predictive models are established. Cutting forces are modelled based on the discretisation concept and an inverse identification methodology. Afterwards the prediction quality is compared to the prediction realised with a predictive model frequently used. The main conclusions are:

- The $R_{c,c}^o$ radius seems to have a significant effect on cutting forces, in the case of an acceptable worn cutting edge. Cutting forces increase when the $R_{c,c}^o$ radius grows.
- The tool wear promotes the $R_{c,c}^o$ radius effect on cutting forces.
- It looks that the $R_{c,c}^o$ radius affects ploughing mechanisms during the material cutting.
- Based on these conclusions, two new models are formalised, according to phenomenological approach. These two models take into account the $R_{c,c}^o$ radius and the uncut chip thickness effects.
- The results provided by the two suggested models underline a major improvement on cutting forces prediction, by reducing from, at least, 19% average modelling relative errors on F_p and F_f components.

This advance allows a fine prediction of cutting forces components, which is crucial in contour turning of complex parts. Indeed, implemented in deformations simulation software, it will help to guarantee that the final part geometry is in respect with geometrical specifications. And so, it avoids highly-cost rejected parts.

Acknowledgments

The authors would like to thanks the SAFRAN group for their technical and material supports given to this study.

References

[1] M.E. Merchant, 2004, Mechanics of the Metal Cutting Process. I. Orthogonal Cutting and a Type 2 Chip, J. Appl. Phys., 16, pp. 267–275.

[2] E.J.A. Armarego, 2000, The Unified-Generalised Mechanics of Cutting Approach - a Step Towards a House of Predictive Performance Models for Machining Operations, Proc 3rd CIRP Int Workshop Model. Mach. Oper., 4, pp. 6–24.

[3] R.G. Reddy, R.E. DeVor, S.G. Kapoor, 2001, A mechanistic force model for combined axial–radial contour turning, Int. J. Mach. Tools Manuf., 41, pp. 1551–1572.

[4] T.H.C. Childs, 2006, Friction modelling in metal cutting, Wear., 260, pp. 310–318.

[5] P. Albrecht, 1960, New Developments in the Theory of the Metal-Cutting Process. Part I: The Ploughing Process in Metal Cutting, Trans. Am. Soc. Mech. Eng., 82, pp. 348–358.

[6] C.-F. Wyen, K. Wegener, 2010, Influence of cutting edge radius on cutting forces in machining titanium, CIRP Ann. - Manuf. Technol., 59, pp. 93–96.

[7] C.K. Ng, S.N. Melkote, M. Rahman, A. Senthil Kumar, 2006, Experimental study of micro- and nano-scale cutting of aluminum 7075-T6, Int. J. Mach. Tools Manuf., 46, pp. 929–936.

[8] R. Stevenson, 1998, The measurement of parasitic forces in orthogonal cutting, Int. J. Mach. Tools Manuf., 38, pp. 113–130.

[9] A.V. Popov, A.V. Dugin, 2012, Experimental methods of determining the cutting forces at the tool's rear surface, Russ. Eng. Res., 32, pp. 68–69.

[10] A. Popov, A. Dugin, 2013, A comparison of experimental estimation methods of the ploughing force in orthogonal cutting, Int. J. Mach. Tools Manuf. 65, pp. 37–40.

[11] A. Popov, A. Dugin, 2014, Effect of uncut chip thickness on the ploughing force in orthogonal cutting, Int. J. Adv. Manuf. Technol., pp. 1–9.

[12] Y. Huang, S.Y. Liang, 2003, Force modelling in shallow cuts with large negative rake angle and large nose radius tools - application to hard turning, Int. J. Adv. Manuf. Technol., 22, pp. 626–632.

[13] M. Kaymakci, Z.M. Kilic, Y. Altintas, 2012, Unified cutting force model for turning, boring, drilling and milling operations, Int. J. Mach. Tools Manuf. 54–55, pp. 34–45.

[14] D. Germain, 2011, Développement d'un modèle d'efforts de coupe intégrant le contact en dépouille : application au tournage de superfinition du cuivre Cu-c2, Arts et Métiers ParisTech.

[15] S. Campocasso, J.-P. Costes, G. Fromentin, S. Bissey-Breton, G. Poulachon, 2013, Improvement of Cutting Forces Modeling Based on Oriented Cutting Tests, Procedia CIRP. 8, pp. 206–211.

[16] ISO 3002-1, 1993, standard.

[17] NF E66-520-4, 1997, standard.

[18] ISO 3685, 1993, standard.

[19] E.J.A. Armarego, C.J. Epp, 1970, An investigation of zero helix peripheral up-milling, Int. J. Mach. Tool Des. Res., 10, pp. 273–291.